REVIEW OF THE AERODYNAMICAL LOAD ON A DUAL-ROTOR WIND TURBINE'S BLADE

IKERSZÉLTURBINA LAPÁTJAIN ÉBREDŐ AERODINAMIKAI TERHELÉSEK VIZSGÁLATA

HETYEI Csaba[1] – SZLIVKA Ferenc[2]

Abstract

In our article, we review the traditional wind turbines and non-traditional wind turbines. Then we described the turbine design process based on the available literature, highlighting the mechanical design criteria with the structural loads. Subsequently, a horizontal axis counter-rotating dual-rotor turbine (CO-DRWT) and a horizontal axis single-rotor wind turbine (HAWT) were compared by computational fluid dynamics simulation (CFD).

Based on our simulation, we were examining the forces on the blades of the two-rotor turbine and their components, we found that the residual force on the blades is higher and more complex, therefore, the possibility of fatigue is more likely. A dual-rotor wind turbine has a life and it requires more frequent condition diagnostics and maintenance.

Keywords

CFD, Fatigue, FEM, Fluid dynamics, Operational safety, Simulation, Solid mechanics, Wind turbine

Absztrakt

Cikkünkben áttekintettük a tradícionális szélturbinákat és a nemtradícionális szélturbinákat. Ezt követően ismertettük a rendelkezésünkre állós irodalom alapján a turbinatervezés folyamatát, kiemelve a gépészeti tervezést és az ott ébredő szerkezeti terheket. Ezt követően numerikus áramlástani szimulációval (CFD) összehasonlítottunk egy vízszintes tengelyű ikerturbinát (CO-DRWT) és egwy vízszintes tengelyű egyrotors turbinával (HAWT).

Szimulációnk alapján a kétrotoros turbina lapátjain ébredő erőket és azok komponenseit vizsgálva megállapítottuk, hogy a lapátokon ébredő erők eredője nagyobb, erőrendszere komplexebb, így a kifáradás lehetősége valószínűbb, mely rövidebb élettartamot és gyakoribb állapotdiagnosztikát és karbantartást igényel.

Kulcsszavak

CFD, Folyadékok mechanika, Kifáradás, Szilárdtest mechanika, Szélturbina, Szimuláció, Üzembiztonság, VEM

[1] hetyei.csaba@phd.uni-obuda.hu | ORCID: 0000-0003-2915-4540 | PhD student/doktorandusz | Óbudai Egyetem Biztonságtudományi Doktori Iskola

[2] szlivka.ferenc@bgk.uni-obuda.hu | ORCID: 0000-0002-3298-4142 | Professor/egyetemi tanár | Óbudai Egyetem Bánki Donát Gépész és Biztonságtechnikai Mérnöki Kar

INTRODUCTION

Nowadays fear from the nuclear accident and the environmental damage, renewable energy sources become more and more into the focus. One of these energy sources the wind energy which was used until the beginning of the civilization for sailing and milling. The first example of a windmill which was used for flour grinding was the Nastifan. This ancient engineering machine was built in the 9th century, three centuries earlier than the first known windmills appear in north-western Europe [1]. The Nastifan Windmill was a vertical axis windmill, its reconstructed version is shown in Figure 1.

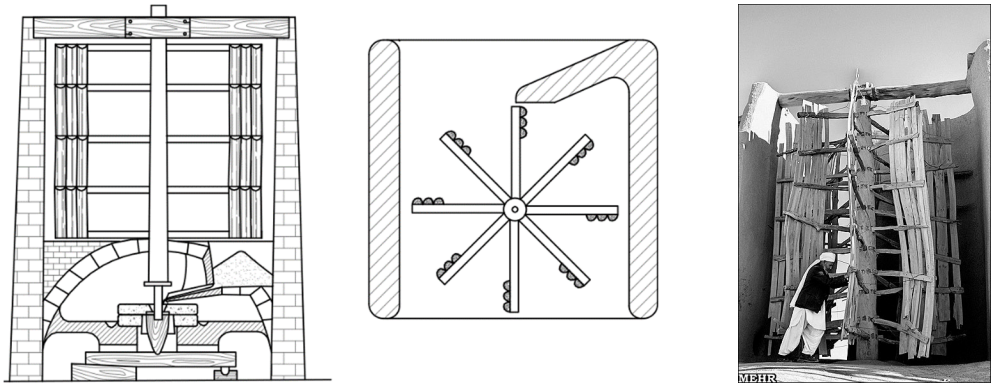

Figure 1.: Conceptual outline and reconstructed version of Nashtifan Windmill [2]

The European windmill which we know as the "Dutch Windmill" was a horizontal axis windmill, which has a long history until the American Windmill, the first modern windmill was invented by Daniel Halladay in the middle of the 19th century.

Using the existing design and knowledge after three decades of the invention of the American Windmill, the first vertical axis wind turbine (VAWT) was invented in 1887 by James Blyth and the first horizontal axis wind turbine (HAWT) was invented in 1888 by Charles Brush. This two turbine is shown in Figure 2.

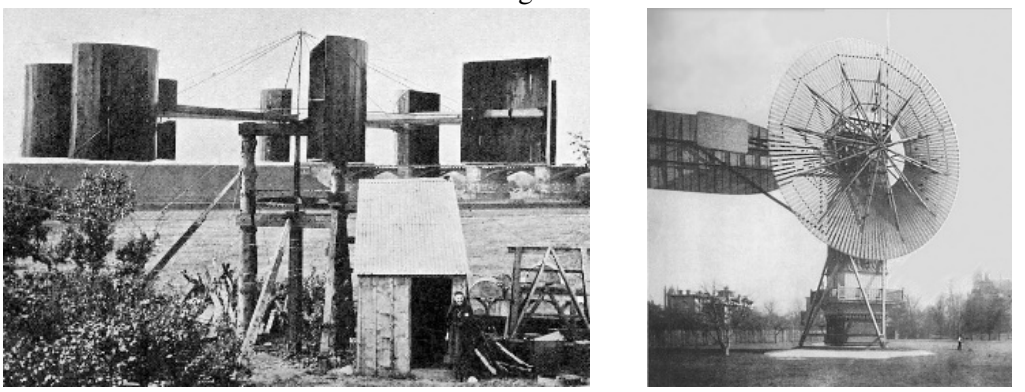

Figure 2.: James Blyth's VAWT (left) and Charles F. Brush's HAWT (right) [3, 4]

After the first VAWT and HAWT, the development of the wind turbines is increased and the turbines start to spread on the globe. The 70's and 80's oil crisis push in the developments and the number of the installation. Nowadays, fear from the nuclear accident and the environmental damage, the wind turbine (WT) installation progressively starts growing. This process can be seen in the global statistics, for example in BP's 2019 report [5], which can see in the next figure.

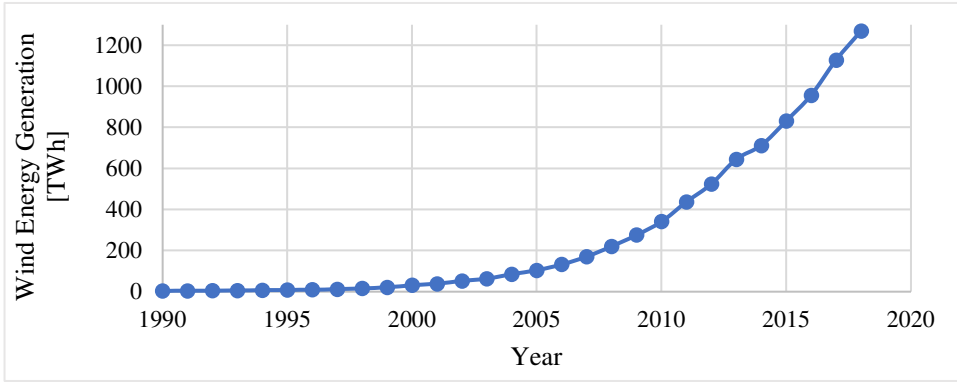

Figure 3.: Wind energy generation globally by year in Terawatt-hour [5]

The growing use of WTs has produced a new variety of appearance, which category is the unconventional wind turbines. This kind of turbines is any new type which has a parameter or property which alters from the 90's or the early 2000's design. One of them is the Archimedes Screw Wind Turbine, which can operate with low noise as a result of its relatively low rotational speed. This Archimedes Screw WT is shown in Figure 4.

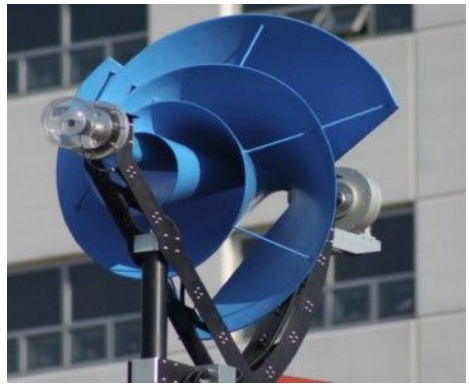

Figure 4.: Unconventional WT: Archimedes Screw Wind Turbine [6]

Other examples for the unconventional WTs are the dual rotor wind turbines, which has two rotors. This type of WTs has two subcategories according to the direction of rotation, these are the co and counter-rotating dual-rotor wind turbines. When the geometry of the turbine are mirrored and the rotors are rotating in the opposite direction they are the counter-rotating dual-rotor wind turbines (CO-DRWT). When the geometry is the same and

the rotors rotate in the same direction, they are the co-rotating dual-rotor wind turbines (CR-DRWT).

Figure 5.: Unconventional WTs: Dual-Rotor Wind Turbine

The first theory about the single rotating wind turbines (SRWT) efficiency was made by Betz in 1919. The Betz's model predicts the power coefficient (c_p), which is the efficiency to 16/27 (59.259%) in an idealized world, where there is no any kind of loss factor, and the turbine is independent of the geometry and it has an infinite number of blades. By the GGS model [8] from 2001, which is a curvilinear model against the rectilinear Betz model, the c_p's maximum value is 30.113%. By measurements, the WTs' power coefficient usually between these two limits.

Theoretically, with the known maximum performance the SRWT's maximum load can be calculated. In the next two chapters, we will review the foundation of the wind turbine's design and the basics of the fatigue failure, then with the use of a CFD (computational fluid dynamics) software, we will determine the aerodynamical load of a CO-DRWT, which can be used for an FEA (finite element analysis) software to establish the stress and the durability.

THE BASICS OF WIND TURBINE'S DESIGN

The wind turbines are complex electro-mechanical systems which have multiple design conditions in the mechanical side as well in the electrical side and IT side. In this paper, we will focus just the structural loads, the internal loads of the working mechanical and electrical component will not be detailed.

The mechanical design usually starts with the structural design of the rotor and tower, then it is followed by the aerodynamic design, where the aerodynamic loads are derived. The structural design seeks the optimum of strength, weight, and cost, the aerodynamic design main goals are the optimum of efficiency, noise reduction (if it's needed, e.g. for onshore turbines or for small WTs that can be installed on buildings), and cost [9]. The requirements of a WT design shown in Figure 6.

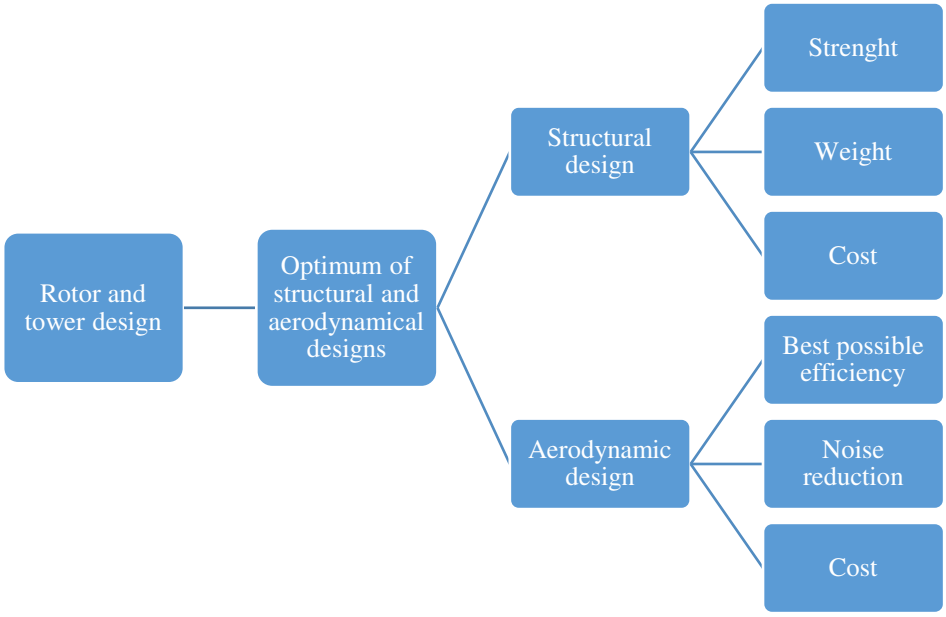

Figure 6.: Design requirements for a wind turbine [9]

The wind turbines failure can occur for four reasons, 1. Extreme wind; 2. Inadequate control system; 3. Collision with birds, UAVs, and other flying objects; and 4. Cyclic-load fatigue which may lead to material fatigue.

The first three reasons will not be explained in this article. The fatigue is an important topic since wind turbines are designed to operate at least 20 years, within the rotor rotates more than 10^9 revolutions. In every rotation, the loads are repeated, which lead to material changing example strain hardening or brittle fracture.

For the HAWT the most relevant loads are the 1. aerodynamic loads; 2. control loads; 3. dynamic loads; and 4. gravitational loads.

The aerodynamic loads are the lift and drag forces, and the momentum which can be predicted with the blade element momentum (BEM) theory. The control loads origins are the blade pitch angle control which is why the torque is used to continuously change for the optimal tip-speed ratio. The dynamic loads are related to the blade's motion, for example, the centrifugal force or the gyroscopic loads. The gravitational loads are associated with the weight of the blade, example the self-weight which is altering by the rotational angle or the eccentricity which due to the deformation in wind load, or due to the manufacture and assembly… [9]

The listed forces also load the tower as well as the blades. The tower is usually a cylinder with decreasing cross-section, in contrast, the blades are multi-component parts. The parts are the 1. airfoil skin; 2. spam flange; 3. shear web, and 4. adhesive. The structural function of the airfoil skin is to provide edge-wise torsional stiffness, the spare flange has to support the flap-wise bending stiffness and the buckling resistance, the shear web or webs have to handle the shear stiffness, and the adhesive must ensure structural integrity. By the

number of shear webs, the blade structures are divided into chambers, a three-chamber airfoil structure shown in Figure 7.

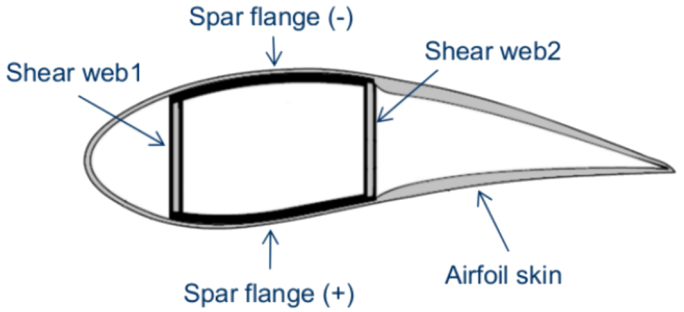

Figure 7.: Cross-section of a 3 cell airfoil structure [12]

For the sections structure design, the two main requirements are to be stiff and lightweight. Lin *et al.* [13] was creating a mathematical model for calculating the cross-section of a multiple composite layer airfoil with one to three-chamber. Heo *et al.* [14] analysed with FSI (fluid-structure interaction) a three cell airfoil structure with chiral, regular and re-entrant hexagonal honeycombs cellular cores under a static load through the deformation. They airfoil cross-sections are shown in the next figure.

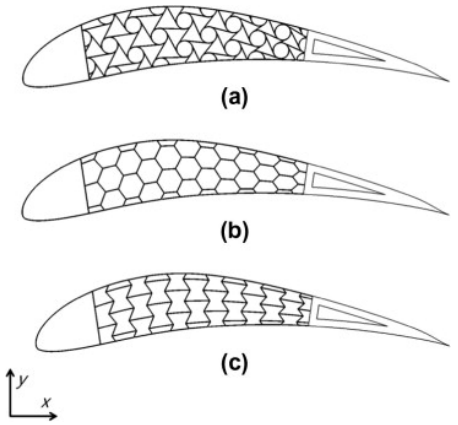

Figure 8.: Analysed airfoil sections of Heo et al.*:*
(a) chiral honeycomb, (b) regular and (c) re-entrant honeycombs [14]

The rotor's blade can be modelled as a cantilever beam, where for each section the BEM theory provide the loads for the segment as it is shown for a *dx* segment on Figure 9.

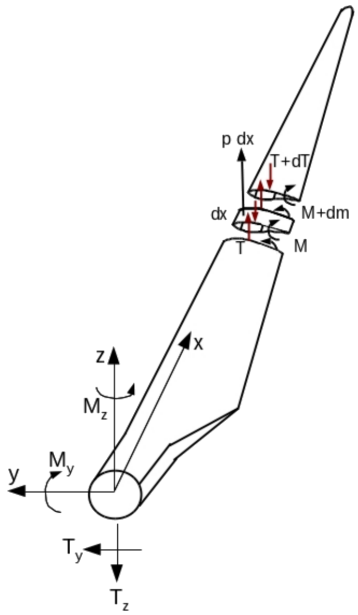

Figure 9.: Shear forces and moments on the root of the blade and a dx long segment [9]

In the previous figure, T_i and dT are the shear forces, M_i and dM are the moments in the x-y-z coordinate system, and p is the residual force on the segment.

The deformation which occurs on the blade can be calculated analytically as we mentioned previously and numerically like Cox presented [12] in his study. On the other hand, laboratory testing with small scale model can predict the deformation and the forces on the 1:1 scale turbine, and the on-site measurement can clarify the simulated and predicted loads and deformation. Example Ovenden *et al.* [15] had a strain gauge and a laser displacement measurement to detect the blade faults. The laboratory experiment showed the strain gauge measurement was more precise, and the laser displacement sensor was able to detect misalignment and bolt loosening. This built-in system can extend the currently running SCADA (supervisory control and data acquisition) system of the WTs. Small and medium-sized wind turbines, where a complex SCADA system and its sensors are not required by economic reasons and by internal space requirements, or for old large-scale turbines which control and data acquisition systems are insufficient and the upgrade is not possible Nagy and Ingo [16] designed an unmanned flying platform (UAV) with a data acquisition system (DAQ). This system was able to measure ambient temperature, humidity, pressure, wind speed and direction, spatial position with high accuracy, and distance with range sensor. If the UAV extended with a DAQ and an image acquisition system for measuring fluid dynamic parameters and analysing graphically the blades of the WTs a high speed and reliable communication system is required. Huszák [17] designed a GPS based automatic UAV antenna tracker system which can be used between a continuously moving UAVs and their ground control system.

BASICS OF FATIGUE FAILURE

With a better and more detailed analytical and numerical tool and with their validating measurements, loads of the components of a WT can be described more precisely. Knowing the generated forces and the component failure process a malfunction is more predictable. When the wind turbine blades have a failure, which is not a collision with an unattended fling object or it does not the cause of an overload or a malfunction of the control system, it is the fatigue failure.

The first stage of the fatigue failure progress, when cyclic-load damages the microstructure of the blade and it create new crack nucleations. On the second stage, the existing micro-crack (by the damages or by the manufacturing) start growing and a "short" discontinuity arises. On the third stage, a "large" crack growing until the fourth and final stage, when the ultimate failure occurs. These stages are shown with their theoretical cycle number in Figure 10.

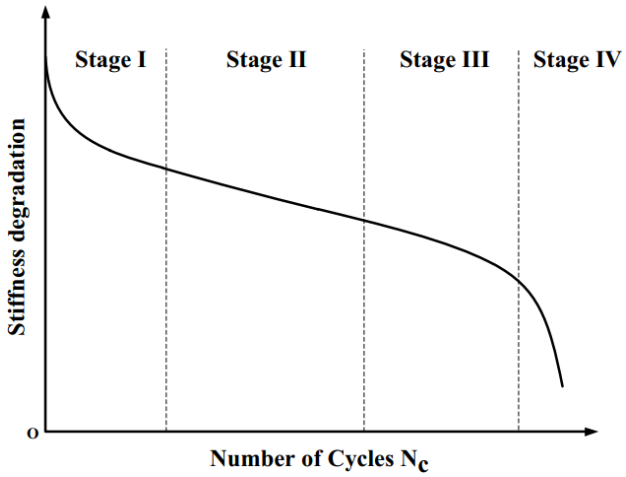

Figure 10.: Four stages of the fatigue failure process [18]

Depending on the material and the stress ratio, the critical number of cycles are changing. For some blade material an S-N curve (Wöhler curve), which is the alternating average stress against the number of load cycle shown in the next figure (Figure 11).

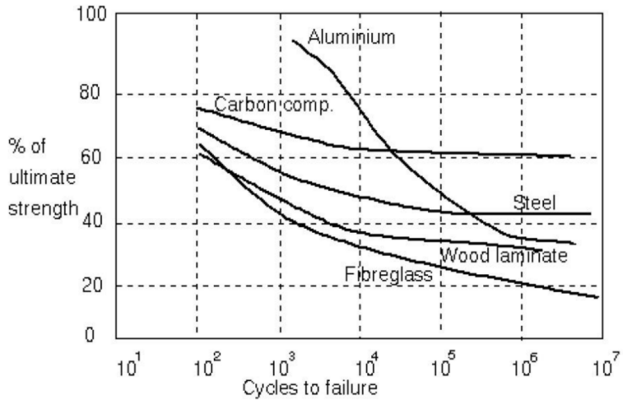

Figure 11.: S-N curves for blade materials [19]

In the previous figure, the ultimate strength was used as a failure parameter besides, other parameters can be used for stiffness degradation e.g. the dislocation density.

The blade structure has different material for a different purpose, the shear web usually made by aluminium or a highly alloyed lightweight steel. The airfoil skin is generally high-strength composite materials, such as fibres (glass-carbon, aramid-basalt, natural and hybrid composites) with thermosets (epoxies, polyesters, vinylesthers), thermoplastics or nanoengineered polymers matrix. Usually, adhesive bonding is carried out the connection between the shear web and the airfoil skin.

The fatigue of the wind turbine blades is a known failure process, Chen *et al.* [21] have a preliminary full-scale (52.3 m long) blade test, where they found during the physical tests the blade exhibited multiple failure modes e.g. laminate fracture, delamination, sandwich skin-core debonding, sandwich core failure, and shear web fracture. Lee *et al.* [22] presented an experiment and a finite element study in their paper, where they find a delamination failure at the end of the wind turbine blade root. Ghasemnejad *et al.* [23] was testing composite materials post-buckling failures.

Noda and Flay [24] were written a fatigue estimation program for HAWTs. Repetto and Torrielli [25] have a used simulation with a rainflow-counting algorithm for 50 years wind-induced fatigue loadings of a slender steel structure (lightning pole) which can be used for wind turbine tower. Repetto and Torielli's long-term simulation includes a mean wind speed combined with short-term wind fluctuation due to the turbulence. Jang *et al.* [26] presented a fatigue life prediction method, where Yang *et al.* developed a fatigue stress spectrum for fatigue critical locations and they have estimated the fatigue life of a blade.

CAD AND SIMULATION PARAMETERS

For having the aerodynamical loads, we had to create a 3D CAD model, where the first turbine rotor was mirrored and used for the second rotor and they rotated in opposite direction. The rotors were connected with a cylindrical nacelle. The diameter of the rotors was 1800 mm, for the root sections FFA-W3-211, to the middle sections S807 and for the tip section, NACA 63-215 airfoils were used. CAD geometry is shown in Figure 12. The

distance between the two rotors was 450 mm which is 0.25D distance (D denotes the rotor diameter).

The twist angle and the radius vs. chord length shown in Figure 13. For clarity, the cord length of the first section (at R = 0 mm) was 71.998 mm and the ratio is 0, which can see in the figure.

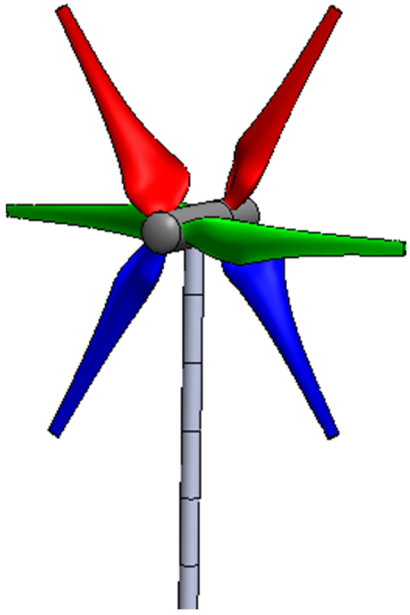

Figure 12.: CAD model of CO-DRWT (self-editing)

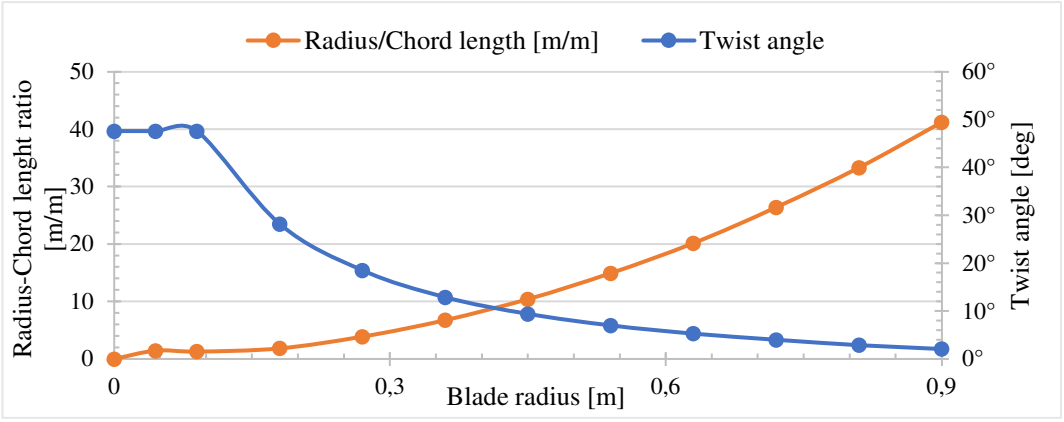

Figure 13.: Chord length and twist angle of the blade (self-editing)

The tower height was 2 000 mm with a constant 70 mm diameter. The external face of the tower was divided with 250 mm segments for evaluation purpose. The tower was halfway from each rotor.

For the simulation, Mentor Graphics' FLOEFD was employed with a rectangular computational domain, which is shown in Figure 14.

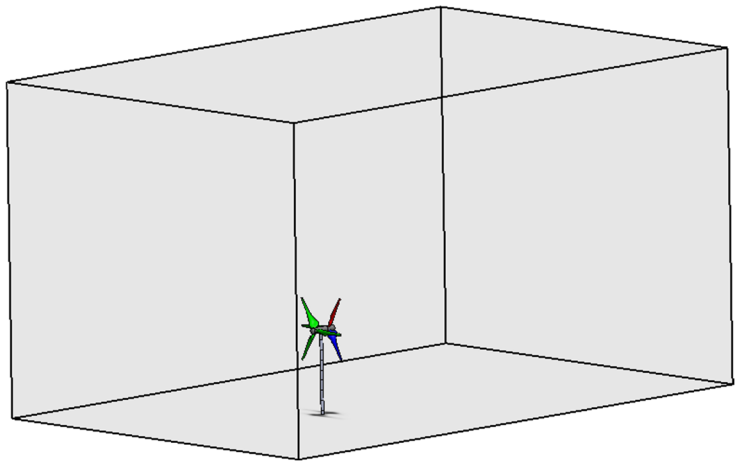

Figure 14.: Computational domain ()

The domain sizes were 5.5D x 4.65D x 8.35D. The domine started 3.225D before the centre of the tower and ended after the tower's centre with 5.125D. The bottom of the tower was aligned with the bottom of the computation domain. The centre of the tower was in the middle of the width of the domain.

The air entered at the beginning of the domain, the other five faces have an environment pressure boundary condition, where the air could enter and exit from the domain. The turbines rotational speed was 20 RPM.

K-ε turbulence model was used with a two-scale wall function based on the Van Driest model.

For computing resource efficiency, we started our simulation from steady-state as an initial condition, then we continued the study until 7.25 seconds. For meshing, we used a basic mesh for steady-state and the same for transient simulation until the 0.5 seconds, where the adaptive meshing finer automatically the initial grid till 1 500 000 elements.

For comparison purpose, we created an SRWT (single rotor wind turbine) model with the same simulation parameters.

RESULTS

After each simulation, we have a pressure distribution on the surfaces as well in the sections of the domain. The pressure distribution of the two configurations shown in Figure 15.

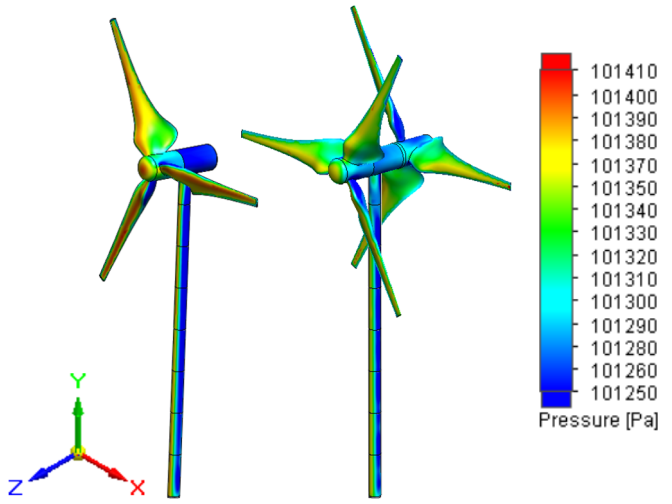

Figure 15.: Pressure distribution on the turbines (self-editing)

On the pressure distribution we can establish, the pressure on the front face where the flow reaches the body higher than on the back faces due to the dynamic pressure.

The velocity filed for steady-state cases shown in the next figures (Figure 16 and Figure 17). From both results we can establish, the wind velocities increase near the blades, and back to the wind turbines and the towers in the wake region, the velocities are slowed down. Also, we can state the CO-DRWT have a larger wake than the SRWT. In the transient simulations, the flow filed depend by the time, therefore the higher and lower velocities are fluctuating hence the turbulency and we can see the vortex shedding at the tip of the blades.

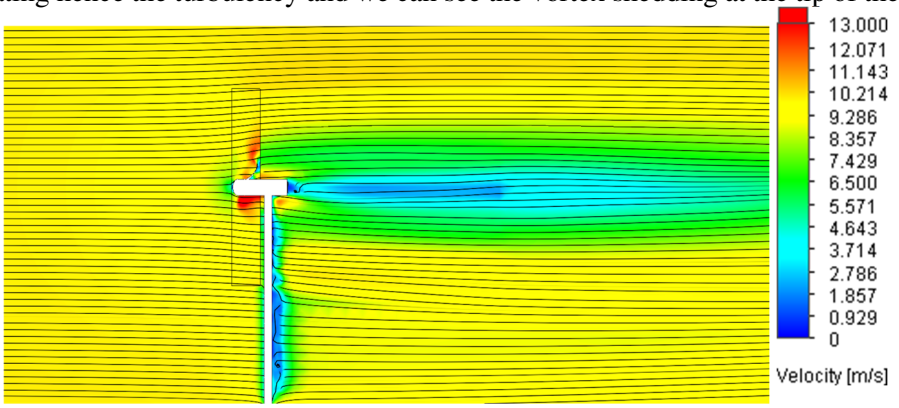

Figure 16.: Velocity distribution in the region of SRWT (from steady-state)

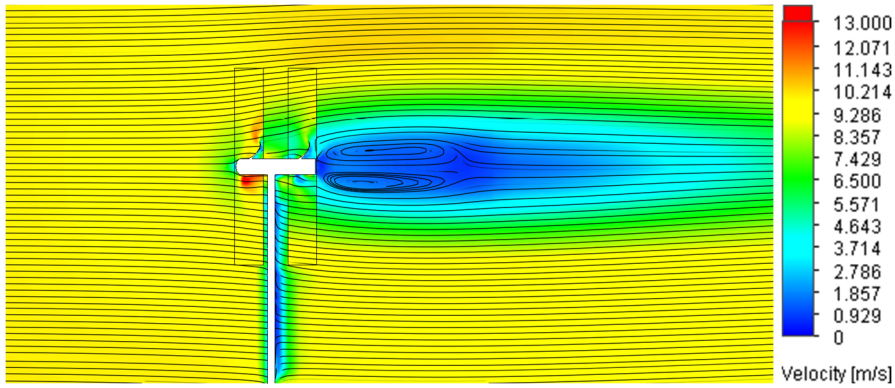

Figure 17.: Velocity distribution in the region of CO-DRWT (from steady-state)

The simulations started with an initial coarser mesh until 0.5 second where the adaptive mesher of the FLOEFD was finer the grid. After the adaptive re-meshing, the flow field should be relaxing for a couple of iterations, therefore we chose 1 second to start our evaluation.

For evaluation, we were numbering the blades and the tower's sections, which are shown in Figure 18. For evaluation, we choose the Blade 1 (marked with red colour) from each rotor and the tower's second and third section (marked with mustard yellow colour). The indications were likewise for SRWT.

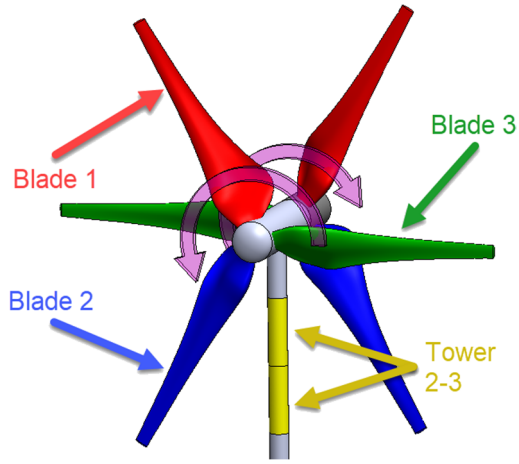

Figure 18.: The numbers of the blade and tower sections (self-editing)

In the next figure (Figure 19) the aerodynamical forces are shown on Blade 1.

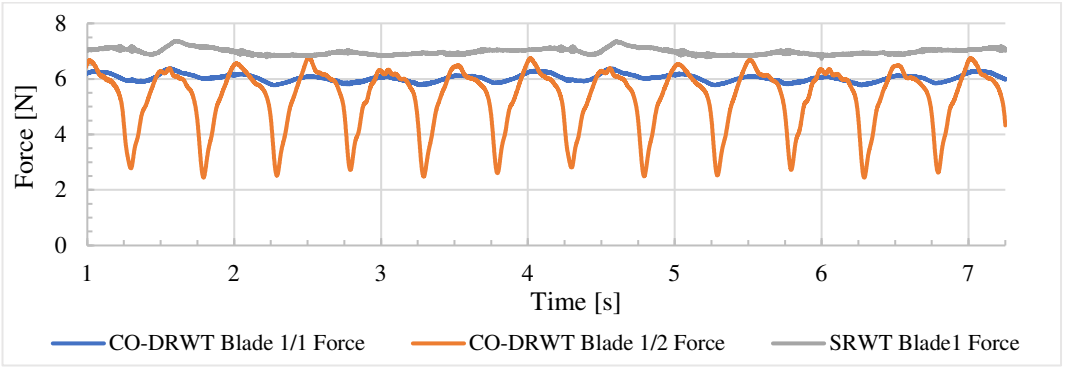

Figure 19.: Aerodynamical force on the surface of Blade 1 (self-editing)

Using the coordinate system of Figure 15, the X component of the aerodynamic forces on Blade 1 is shown in Figure 20.

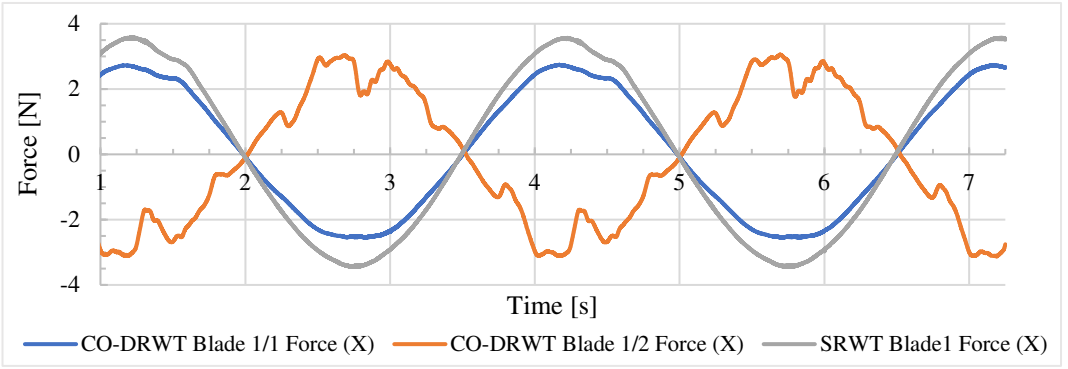

Figure 20.: X component of the aerodynamic force on the surface of Blade 1 (self-editing)

Using the coordinate system of Figure 15, the Y component of the aerodynamic forces on Blade 1 is shown in Figure 21.

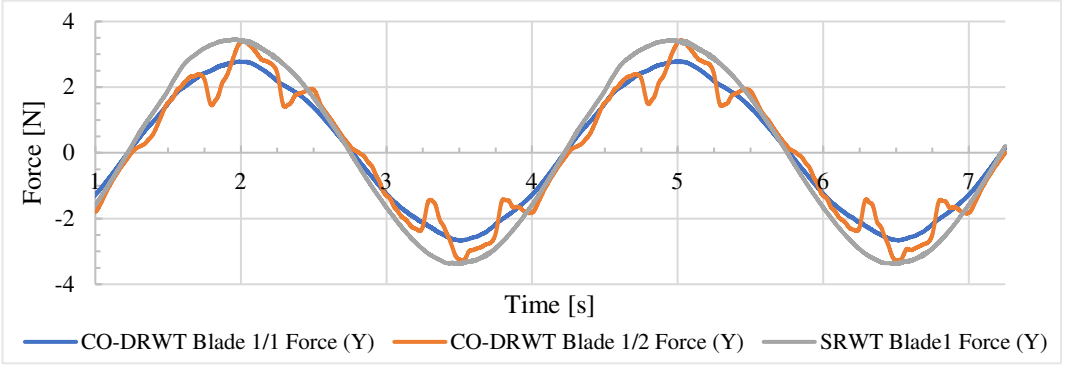

Figure 21.: Y component of the aerodynamic force on the surface of Blade 1 (self-editing)

Using the coordinate system of Figure 15, the Z component of the aerodynamic forces on Blade 1 is shown in Figure 22.

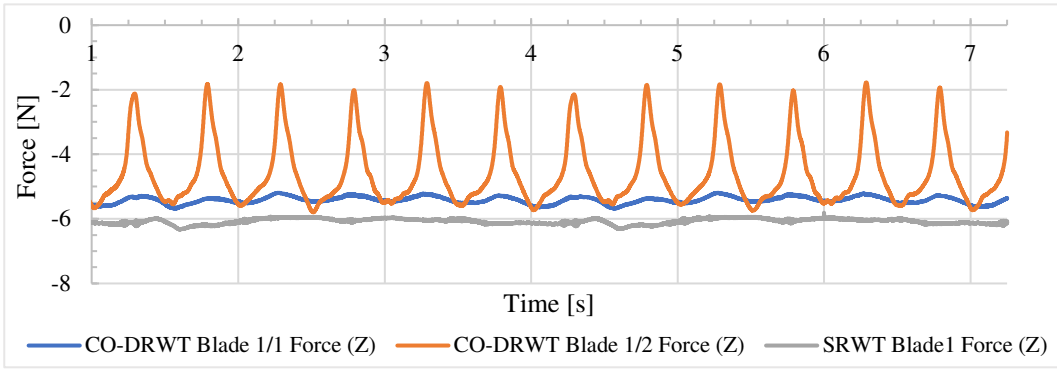

Figure 22.: Z component of the aerodynamic force on the surface of Blade 1 (self-editing)

The residual force on the tower's second and third sections shown on Blade 1 in Figure 23.

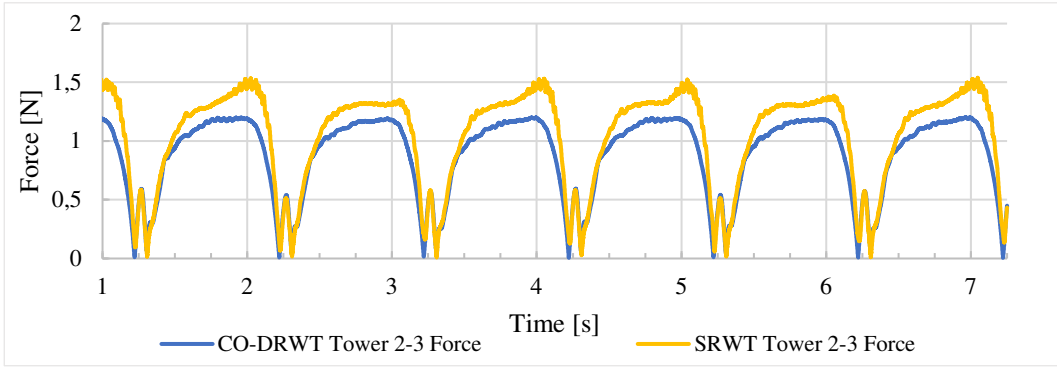

Figure 23.: The residual aerodynamical force on the tower's second and third sections (self-editing)

The component of the residual aerodynamical force on the tower's second and third sections is shown in Figure 24.

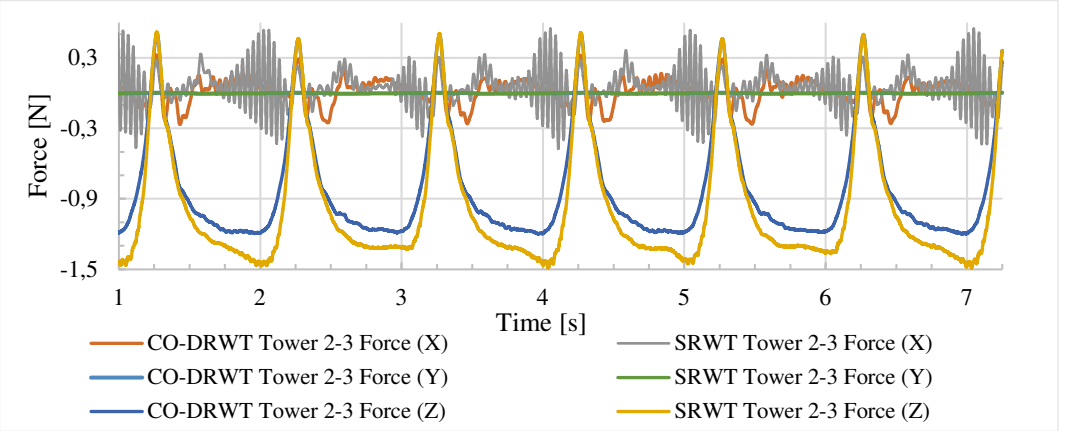

Figure 24.: The X, Y, and Z component of the aerodynamic force on the tower's second and third sections (self-editing)

Based on the results, the following can be stated:

1. On the blades of the SRWT's rotor, the aerodynamic force is higher, than on the blades of the CO-DRWT's first rotor (Blade 1/1), but it is less than the overall loads on the CO-DRWT's rotors (see Figure 19).
2. The tower's pass frequency is difficult to see but can be found on the parameters (e.g. aerodynamic force) of the SRTW's blades.
3. The rotational speed of the rotors was constant 20 RPM, the Blade 1 had to pass in front of the tower at 1.25 sec and further 3 sec later. The trace of the blade-tower interaction can be seen on the aerodynamical load diagrams 0.35 second later than as when it happened, due to the distance between the two surfaces. The Blade 1 of the CO-DRWT's blade has the trace of the blade-tower interaction, approximately in the same moment than the SRWT's first blade, but it is not noticeable, because the Z component of the aerodynamical load is sinusoidal and the minima of the sine are approx. in the same moment with the interaction of the two faces (see Figure 19 and Figure 22).
4. On the blades of the CO-DRWT's second rotor, the trace of the first rotor's blade can be found in every 0.5 seconds (see Figure 20, Figure 21 and Figure 22).
5. The X and Y components of the aerodynamical force on the blades are sinusoidal. The X component of the aerodynamical force on the CO-DRWT's second rotor is shifted with 90° than the first rotor's phase. The Y component of the aerodynamical force on the CO-DRWT's first and second rotor are in sync (see Figure 20, Figure 21).
6. The blade pass frequency can be seen in each second on the forces of the 2nd and 3rd sections of the tower (see Figure 23 and Figure 24).
7. The Z component of the aerodynamical load on the 2nd and 3rd sections of the tower resembled a trapezoid for SRWT and CO-DRWT. By the coordinate system (which

is shown in Figure 12) the Z component is negative in most of the time. When the blades pass in front of the tower the loads change their direction and it's peak value positive. The maximum value for each turbine approx. +0.45 N, the minimum values are near -1.1 N for the CO-DRWT and -1.4 N for the SRWT. The Y component of the aerodynamical load seems to be a random fluctuation, which changed its direction and its value increases near the blade-tower interaction. Contrary to our expectations, the frequency of the load fluctuation is faster to the SRWT, than for the CO-DRWT. The Y component peak values are between -0.042 and +0.5 N for the SRWT, and -0.027 and +0.03 N for the CO-DRWT. The X component of the aerodynamical load resembles a sawtooth wave for each turbine. The X components value for SRWT is between -0.0055 and +0.003 N, for CO-DRWT -0.0045 and +0.0035 N (see Figure 24).

8. For the SRWT the rotational frequency and the tower pass frequency are 1X, the blade pass frequency is 3X, where the X is the frequency of the rotational speed.
9. For the CO-DRWT, the first rotor's rotational frequency is 1X, the tower pass frequency is 3X, and the second rotor's rotational frequency is 6X.

Based on the statements, we reached the following conclusions:

a) As shown in the figures from Figure 19 to Figure 22, loads of the first rotors have the same characteristics just the magnitude is different. The Z component of the aerodynamical force on the first rotors' blade alternating around a non-zero mean force. The X and Y component of the aerodynamical force on the first rotors' blade is sinusoidal and it is alternating around a zero-mean force.
b) By Figure 22, the Z component of the aerodynamical force on the CO-DRWT's second rotor has a 6X frequency component, due to the first rotor's rotation as it was mentioned in Statement 9. The force is altering around a non-zero mean force and its minima are zero or a close zero values.
c) According to Statement 1, the aerodynamical loads of the SRWT are higher, therefore it will reach the fatigue limit earlier than the first rotor of the CO-DRWT.
d) As shown in Figure 20 and Figure 21, the blades of the CO-DRWT's second rotor have a primary load with 1X frequency, which is superimposed with a smaller 6X frequency load.
e) Due to the Conclusion b) and d), the blades of the CO-DRWT's second rotor are exposed to greater fatigue than the first rotor of CO-DRWT or the SRWT's rotor.

SUMMARY

In our study, we described the main loads of a wind turbine, then with a CFD software we were simulating a single rotor wind turbine (SRWT) and for a counter-rotating dual rotor wind turbine (CO-DRWT). Based on our results we were comparing the aerodynamical forces on the turbines and then we analysed the results in terms of the high-cycle fatigue.

In our results, we were able to detect the blade-tower interaction for the SRWT and the blade-blade interaction for the CO-DRWT. The second rotor of the dual rotor wind turbine has in the axial direction (Z component of the aerodynamical load) 6 additional load cycle during one rotation (see Figure 22) and in the two other directions (X and Y components of the aerodynamical load) have 6 smaller cycles which were alternating around the primary load (see Figure 20 and Figure 21). By the 6 additional load-cycle, the blades of the second rotor are exposed to have higher fatigue failure than the blades of the first rotor.

Based on the current and our previous studies [27, 28], a CO-DRWT has a shorter operating time due to fatigue, but at this time it is generating more electricity than an SRWT. The optimum between a shorter life with higher energy density and a longer life with lower energy harvesting capability could be one of the next study's subject.

REFERENCES

[1] Szlivka Ferenc, Molnár Ildikó, "*Víz- és szélenergia hasznosítás (Hydro and wind energy utilization)"*, Edutus Főiskola Kiadó, 2012, https://regi.tankonyvtar.hu/hu/tartalom/tamop412A/2010-0017_10_viz_es_szelenergia/index.html

[2] Nashtifan Windmills, http://historicaliran.blogspot.hu/2012/03/nashtifan-windmills.html (Access Date: 23. 09. 2019.)

[3] *"Blyth's Wind Turbine"*, https://upload.wikimedia.org/wikipedia/commons/1/13/James_Blyth%27s_1891_windmill.jpg

[4] *"Charles F. Brush Wind Turbine"*, https://media2.fdncms.com/clevescene/imager/tilting-at-windmills/u/zoom/2622441/cover-3.jpg

[5] BP, "*Statistical Review of World Energy"*, BP Statistical Review of World Energy, London (UK), p. 50, 2019, https://www.bp.com/content/dam/bp/business-sites/en/global/corporate/pdfs/energy-economics/statistical-review/bp-stats-review-2019-full-report.pdf

[6] *"Bizarre Wind Turbines",* https://cdn.trendhunterstatic.com/thumbs/urban-wind-turbine.jpeg

[7] Romańskia L., Bienieka J., Komarnickia P., Dębowskia M., and Detynab J., *"Estimation of operational parameters of the counter-rotating wind turbine with artificial neural networks",* Archives of Civil and Mechanical Engineering, **17**(4), pp. 1019-1028, 2017, https://doi.org/10.1016/j.acme.2017.04.010

[8] Gorban A. N., Gorlov A. M., and Silantyev V. M., "*Limits of the Turbine Efficiency for Free Fluid Flow",* Journal of Energy Resources Technology, **123**(4), pp. 311-317, 2001, https://doi.org/10.1115/1.1414137

[9] Corke T., Matlis E., *"Wind Turbine Performance, Control and Design - AME 40530 (lecture note)"*, University of Notre Dame, Notre Dame, Indiana, United States, 2018.

[10] Johnson D. A., Gu M., and Gaunt B., *"Wind Turbine Performance in Controlled Conditions: BEM Modeling and Comparison with Experimental Results"*, International Journal of Rotating Machinery, **2016**(3), pp. 1-11, 2016, https://doi.org/10.1155/2016/5460823

[11] Probst O., Martínez J., Elizondo J., and Monroy O., "*Wind turbines"*, *Chapter 5: Small Wind Turbine Technology,* IntechOpen, London, 2011, ISBN: 978-953-51-4506-6, https://doi.org/10.5772/643

[12] Cox K., *"Structural design and analysis of a 10 MW wind turbine blade"*, Deep Sea Offshore Wind R&D Seminar, Trondheim (Norway), 19. January 2012., https://www3.nd.edu/~tcorke/w.windturbinecourse/Watson-Ahumada.pdf

[13] Lin W., Xiongwei L., Lianggang G., Nathalie R., and Matthew S., *"A mathematical model for calculating cross-sectional properties of modern wind turbine composite blades"*, Renewable Energy, **64**, pp. 52-60, 2014, https://doi.org/10.1016/j.renene.2013.10.046

[14] Heo H., Ju J., and Kim D.M., *"Compliant cellular structures: Application to a passive morphing airfoil"*, Composite Structures, **106**, pp. 560-569, 2013, https://doi.org/10.1016/j.compstruct.2013.07.013

[15] Ovenden M., Wang Q., Huang S., Zhao W., and Wang S., *"Real-Time Monitoring of Wind Turbine Blade Alignment Using Laser Displacement and Strain Measurement"*, ASME J Nondestructive Evaluation, **2**(3), 2019, https://doi.org/10.1115/1.4043850

[16] Nagy A., Jahn I., *"Advanced Data Acquisition System for Wind Energy Applications",* Periodica Polytechnica Transportation Engineering, **47**(2), 2019, pp. 124-130, https://doi.org/10.3311/PPtr.11515

[17] Huszár P., *"UAV és földi szegmense közötti kommunikáció hatékonyságának javítása (Improving communication efficiency between UAV and its ground segment)"*, Repüléstudományi Közlemények, **31**(1), pp. 167–182., https://doi.org/10.32560/rk.2019.1.14

[18] Gao X., Koval G., and Chazallon C., *"A discrete element model for damage and fracture of geomaterials under fatigue loading"*, The European Physical Journal Conferences, **140**, 2017, https://doi.org/10.1051/epjconf/201714012018

[19] Ragheb M., *"Fatigue loading wind turbine"* https://mragheb.com/NPRE%20475%20Wind%20Power%20Systems/Fatigue%20Loading%20in%20Wind%20Turbines.pdf

[20] Mishnaevsky L., Branner K., Petersen N. H., Beauson J., McGugan M. and Sørensen, F. B.,, *"Materials for Wind Turbine Blades: An Overview"*, Materials, **10**(11), 2017, https://dx.doi.org/10.3390%2Fma10111285

[21] Chen X., Zhao W., Zhao X. L., and Xu J. Z., *"Preliminary failure investigation of a 52.3 m glass/epoxy composite wind turbine blade"*, Engineering Failure Analysis, **44**, pp. 345–350, 2014, http://dx.doi.org/10.1016/j.engfailanal.2014.05.024

[22] Lee H. G., Kang M. G., and Park J., "Fatigue failure of a composite wind turbine blade at its root end", Composite Structures, **133**, pp. 878-885, December 2015, https://doi.org/10.1016/j.compstruct.2015.08.010

[23] Ghasemnejad H., Occhineri L., and Swift-Hook D.T., *"Post-buckling failure in multi-delaminated composite wind turbine blade materials"*, **32**(10), pp. 5106-5112, 2011, https://doi.org/10.1016/j.matdes.2011.06.012

[24] Noda M., Flay R.G.J., *"A simulation model for wind turbine blade fatigue loads"*, Journal of Wind Engineering and Industrial Aerodynamics, **83**(1-3), pp. 527-540, 1999, https://doi.org/10.1016/S0167-6105(99)00099-9

[25] Repetto M. P., Torrielli A., *"Long term simulation of wind-induced fatigue loadings",* Engineering Structures, **132**, pp. 551-561, 2017, https://doi.org/10.1016/j.engstruct.2016.11.057

[26] Jang Y. J., Choi C. W., Lee J. H., and Kang K. W., *"Development of fatigue life prediction method and effect of 10-minute mean wind speed distribution on fatigue life of small wind turbine composite blade"*, Renewable Energy, **79**, pp. 187-198, 2015, https://doi.org/10.1016/j.renene.2014.10.006

[27] Hetyei Cs., Szlikva F., "*Axial Gap Optimisation of Half Diameter Shifted Counter Rotating Dual Rotor Wind Turbine*", Interdisciplinary Description of Complex Systems, **18**(3), pp. 389-399, 2020, https://doi.org/10.7906/indecs.18.3.9

[28] Hetyei Cs., Szlivka F., *"Rotor size optimisation of a counter-rotating dual-rotor wind turbine",* Biztonságtudományi Szemle, **2**(4), pp. 91-105, 2020. https://biztonsag-tudomanyi.szemle.uni-obuda.hu/index.php/home/article/view/86/103